scientific reports

Check for updates

OPEN

Novel smart window using photonic crystal for energy saving

Zaky A. Zaky & Arafa H. Aly

Smart windows are emerging as an effective way of minimizing energy consumption in buildings. They attracted the major relevance for minimizing energy consumption in buildings. More research studies are needed to design smart windows with operating wide range and don't require additional energy to operate. We suggest a novel smart window structure using photonic crystal to regulate the solar radiation intensity by preventing it from penetrating the buildings in summer. For the first time, the suggested smart window photonic crystal at room temperature is proposed. The suggested smart window can block about 400 nm of near-infrared. This smart window model doesn't require additional heat or electric input to operate.

Switchable electromagnetic wave transmittance using smart windows has recently attracted attention because they are involved in skylights, architectural or vehicle windows, and internal partition applications[1]. Because commercial and residential buildings consume around 40% of overall energy consumption, the implementation of smart windows is of major relevance for minimizing energy consumption in buildings[2]. Heating, air conditioning, and ventilation account for more than half of the total energy consumption[3].

Smart windows control how much ultraviolet (UV), visible, and, most importantly, near-infrared (IR) radiation penetrates buildings. Inside facades, blinds can be used to regulate the solar radiation intensity by preventing it from penetrating the building in summer to reduce the cooling costs. The intercepted solar energy in this traditional way is not being used. Even though Photochromic, electrochromic, and thermochromic materials are chromogenic materials that have been widely used for smart windows to conserve energy, they require additional heat or electric input to operate[4–6].

The dispersion of electromagnetic waves through periodic structures is greatly affected by the photonic band gaps (PBGs). Recently, photonic crystals (PCs) are used in different applications such as filters, biosensors, solar cells, etc.[7–23]. Currently, some advanced spatial smart windows are implemented using the spatial propagation features of traditional PCs[24]. Arafa et al. in 2019 presented a low-temperature smart window using superconductor PC[25]. Blocking or passing the electromagnetic waves in this structure is controlled by changing the incident angle. Also, it can't be used for our buildings because it depends on the usage of superconductor material. It can be used only for low-temperature applications. In 2020, Arafa et al. proposed an optical filter structure to control the propagation of light through it depending on the incident angle[26]. Besides, this structure can't record high (for winter) and low (for summer) transmitted infra-red light at the same time.

The current work is distinct in some ways. For the first time, a detailed simulation study of smart window PC at room temperature is proposed. Moreover, the proposed structure has the ability to block a wide range of IR by filling the air layers with water. It can work at a long range of incident angles. Moreover, the suggested structure doesn't require additional heat or electric input to operate.

Basic equations and materials

Figure 1 presents the proposed smart windows. In the case of Fig. 1A, the visible electromagnetic wave will be transmitted, and IR will be blocked. It is composed of $(SiO_2/Air)^N$ photonic crystal. By filling the cavity layer with water, visible and IR electromagnetic waves will be transmitted as clear in Fig. 1B. N clarifies the number of times the photonic crystal periods will be repeated. The proposed smart windows structure will be deposited on SiO_2 substrate.

SiO_2 layers can be deposited using different techniques such as ion assistance electronic beam deposition[27] and radiofrequency magnetron sputtering[28]. The refractive index of SiO_2 can be calculated by using the following fitted equation[27]:

$$n_{SiO2}(\lambda) = 0.0137\lambda^6 - 0.1286\lambda^5 + 0.4855\lambda^4 - 0.9457\lambda^3 + 1.0055\lambda^2 - 0.5600\lambda + 1.5974, \quad (1)$$

TH-PPM Group, Physics Department, Faculty of Science, Beni-Suef University, Beni-Suef, Egypt. email: zaky.a.zaky@science.bsu.edu.eg

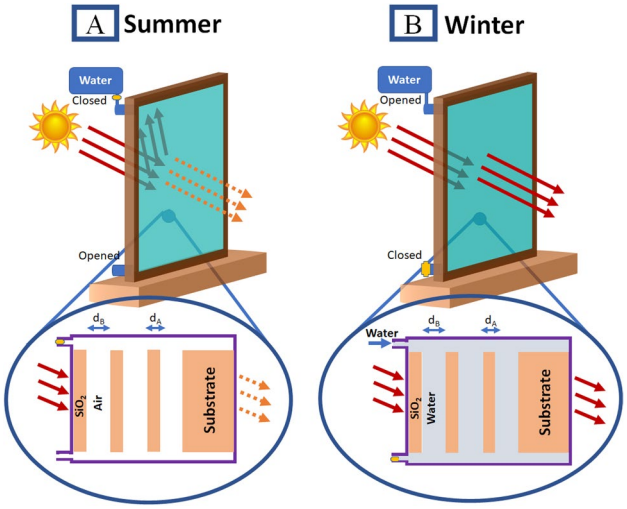

Figure 1. Schematic diagram of proposed smart windows (**A**) in summer, visible electromagnetic waves will be transmitted and IR will be blocked, (**B**) in winter, visible and IR electromagnetic waves will be transmitted.

where λ is the wavelength in μm. We use SiO_2 as a dielectric material because the imaginary part is close to 0 and can be ignored[27]. Zaky et al.[11] cleared a method that can help to control the thickness of Air/water layers during the process of fabrication using the etching process. For certainty, we assume $d_A = 175$ nm, $d_B = 270$ nm, $N = 3$, $n_{Air} = 1$, $n_{water} = 1.33$[29], and $\theta_0 = 0$ degrees as initial conditions.

As the incident sunlight is completely unpolarized, each polarized component (TE and TM components) has its own proper behavior inside the proposed design[30]. The transmittance of the proposed smart windows for TE and TM electromagnetic waves will be calculated by the transfer matrix method (TMM) to investigate how the proposed smart windows react to incident waves[31–34]:

$$T(\%) = 100 * \frac{p_0}{p_s}|t|^2, \tag{2}$$

where

$$t = \frac{2p_s}{(A_{11} + A_{12}p_0)p_s + (A_{21} + A_{22}p_0)}, \tag{3}$$

$$\begin{vmatrix} A_{11} & A_{12} \\ A_{21} & A_{22} \end{vmatrix} = \left(a_{SiO2}a_{Air/water}\right)^N, \tag{4}$$

$$p_k = n_k cos(\theta_k) \text{ for TE} \tag{5}$$

$$p_k = \frac{cos(\theta_k)}{n_k}, \text{ for TM} \tag{6}$$

where θ_k, n_k, a_k, p_0, and p_s are the incident angle of the electromagnetic waves, the dielectric constant, the transfer matrix element, $p_0$and p_s related to air and substrate.

Ethics approval and consent to participate. This article does not contain any studies involving animals or human participants performed by any of the authors.

Results and discussions

To demonstrate the capability of our smart window structure to control the propagation of IR range, we conducted a series of simulation studies using TMM.

For this study, we need a window that lets the visible and near IR range propagate through in winter to warm the buildings internally, and blocks IR in summer. A structure with two conditions will be used for these states, as clear in Fig. 1. In the event that the structure layers are $(SiO_2/Air)^N$, there is a high refractive index contrast between n_{SiO2} and n_{Air}. As a result, a PBG appeared as clear in Fig. 2 (black line). Through the PBG, the intensity of the transmitted IR decreases and reaches a minimum value of 33% at the wavelength of 1053 nm.

By filling the air layers with water as clear in Fig. 1B, the refractive index contrast between the two used layers (n_{SiO2} and n_{water}) strongly decreases. So, the PBG disappeared at the range of wavelength of concern, as clear in

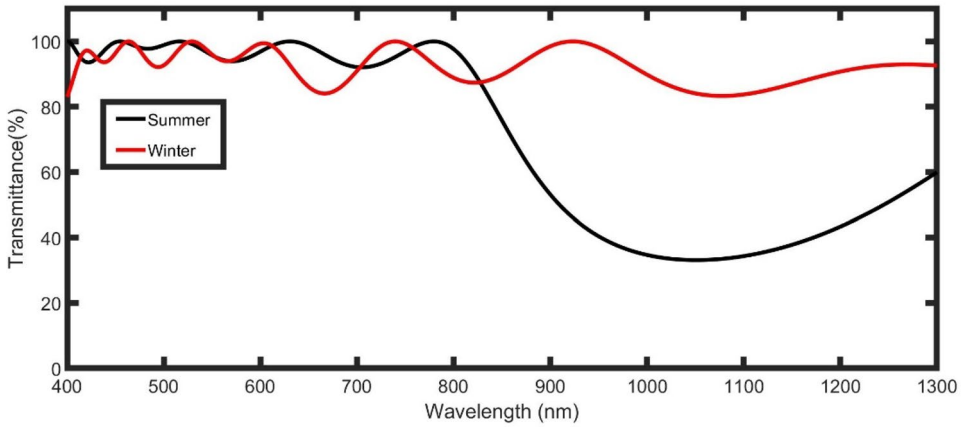

Figure 2. The transmittance of the proposed smart windows for TE polarized light at initial conditions.

Fig. 2 (red line). Then, the structure allows both visible and IR to propagate through it with high transmittance ranging from 90 to 100% and warm the buildings.

In the following studies, we will try to reduce the intensity of IR to achieve a complete blocking as possible as we can. The effect of the incident angle of TE and TM polarized light on the PBG is studied in Fig. 3 for both two conditions (n_{SiO2}/n_{Air} and n_{SiO2}/n_{water}). In order to assess the impact of the incident angle on PBG, the transmittance of the structure versus the wavelength at different incident angles was studied for both TE and TM polarized light.

As clear in Fig. 3A, for the summer structure, the PBG is shifted to lower wavelengths with increasing the incident angle of TE polarized light according to the following relation[35,36]:

$$P = m\lambda = n_{eff}\, G, \tag{7}$$

where P is the optical path difference, m is an integer, n_{eff} is the periodic structure's effective dielectric constant, w is the incoming light wavelength, and G is the geometrical path difference. Since the PBG at the angle of 35 degrees extended from 700 to 1300 nm with a width of 600 nm, this angle is very suitable for the proposed application. Besides, at this angle, a moderated PBG extended from 800 to 1150 nm with a width of 350 nm for TM polarized light, as clear in Fig. 3C.

For winter structure, the angle of 35 degrees also records a suitable visible and IR transmittance for TE polarized light, and high transmittance in the case of TM polarized light, as clear in Fig. 3B,C. So, we recommend this angle in the following studies.

Because the PBG is proportional to the thickness of the used materials, the PBG shifts to higher wavelengths for higher thicknesses of the air/water layer according to Eq. (7). As clear in Fig. 4A,C, with the increase of thickness, the amount of IR with high energies (low wavelengths) can be transmitted for both TE and TM polarized light. So, the thickness of $d_B = 270$ nm will be recommended for the following study.

In Fig. 5, the number of periods will be changed but all other conditions are constants. For the summer structure, the center of PBG seems to be at the same position but the width of the PBG increases and the transmittance decreases. Besides, the edges of the PBG become more vertical and are slightly shifted to higher wavelengths. On the other hand, for winter structure, the transmittance of both TE and TM polarized light slightly decreases.

Where N = 6 has the ability to block much amount of IR in summer, it will be recommended after increasing the incident angle to 40 degrees to adjust the left edge of the PBG at the end of the visible light range and the beginning of IR range. Besides, the transmittance of unpolarized sunlight (blue line) is calculated according to the following equation[30]:

$$T_{unpolarized\ sunlight} = \frac{TE + TM}{2}, \tag{8}$$

It is worth noting that the efficiency of the proposed smart window for blocking TE polarized light is higher than TM as clear in Fig. 6A,B.

Conclusion

We have utilized TMM simulation studies on 1D-PC as a novel smart window at room temperature. This structure recorded high efficiency for blocking a wide range of IR. The results cleared the performance of the proposed smart window and its potential for energy consumption. However, as much or more work remains to be done to improve the efficiency of smart windows to be able to block all ranges of IR and UV for indoor comfort and energy saving.

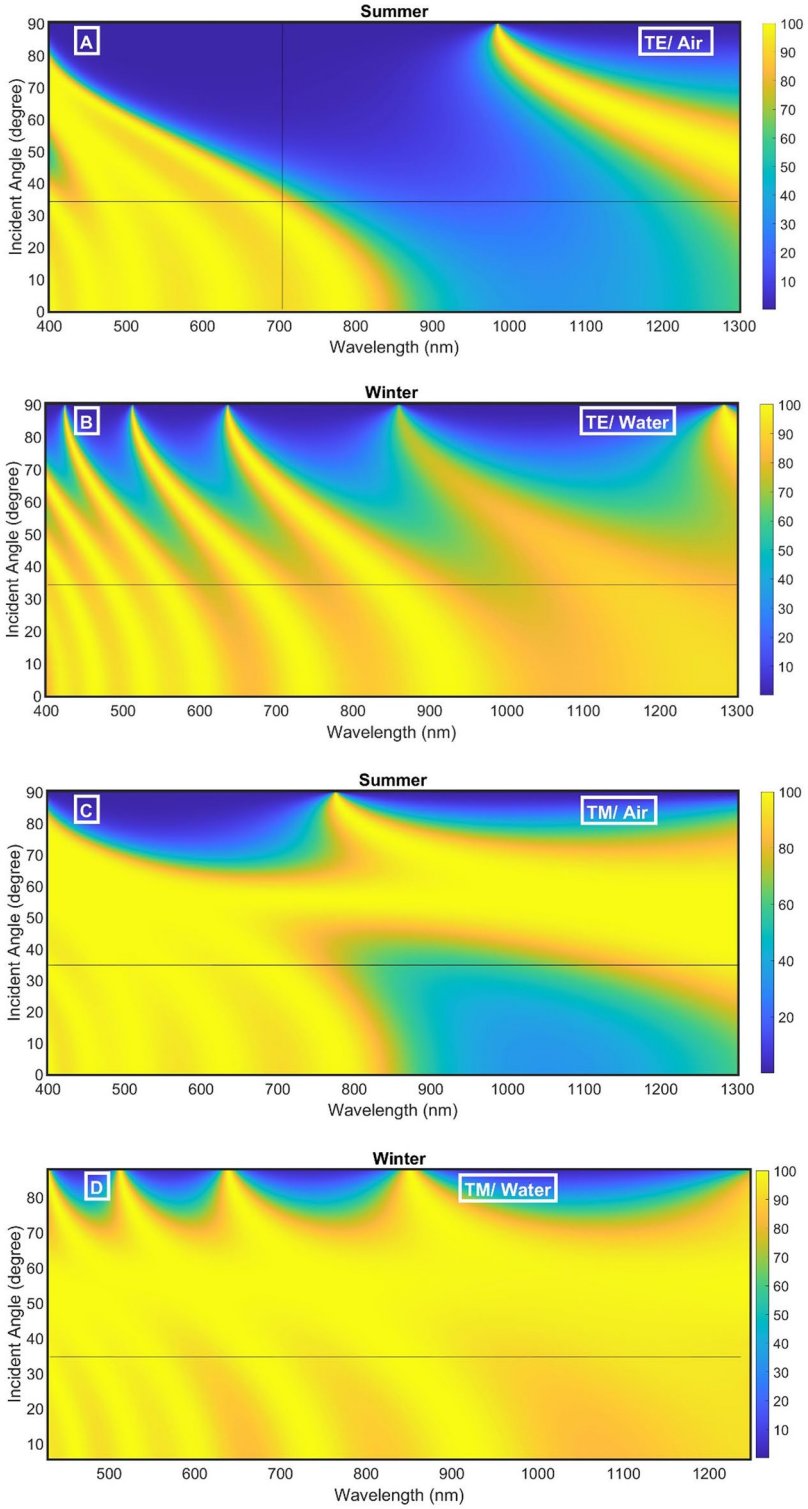

Figure 3. The transmittance of the proposed smart windows at initial conditions as a function of the incident angle (**A**) TE/Air, (**B**) TE/water, (**C**) TM/Air, and (**D**) TM/water.

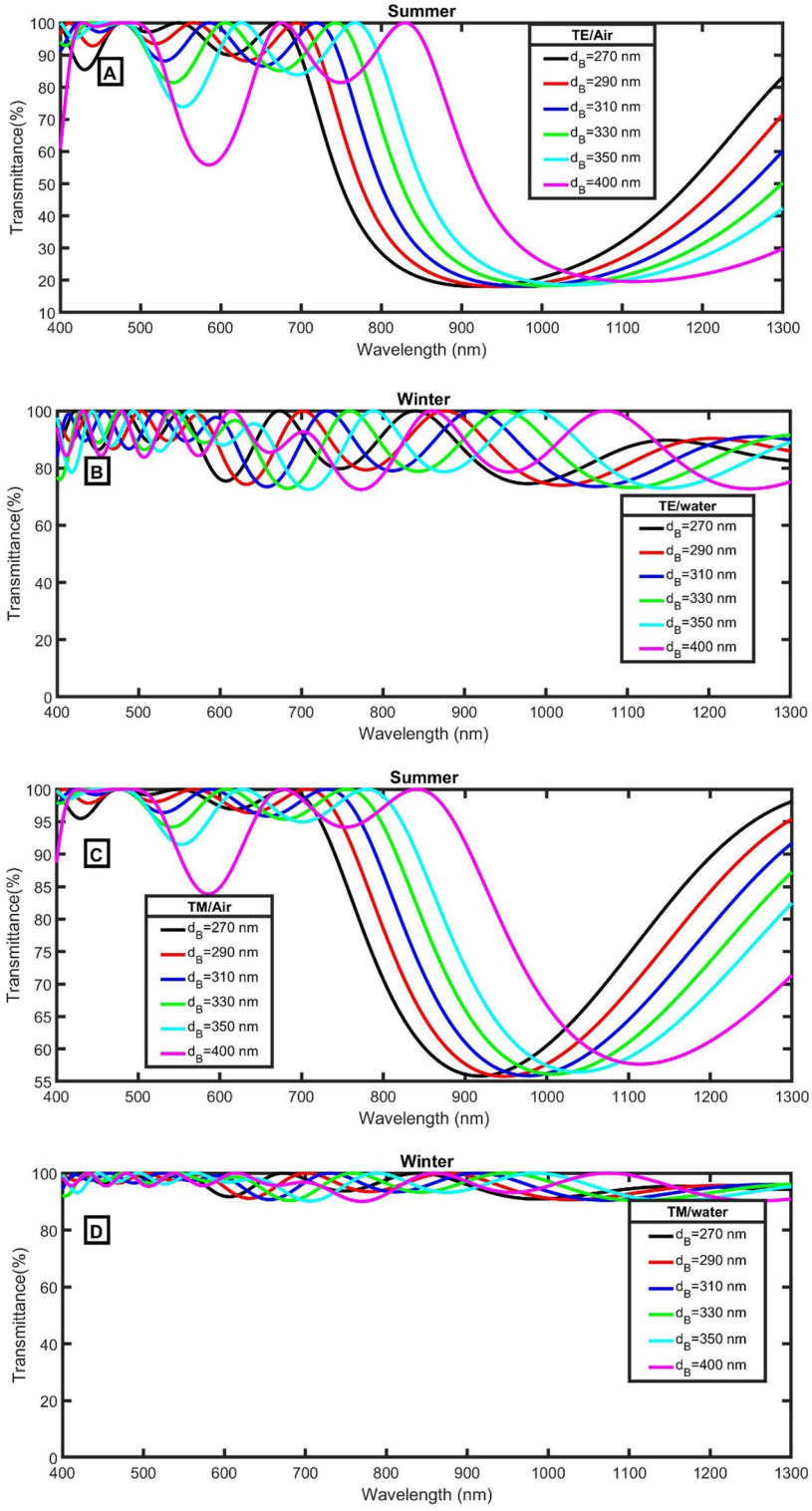

Figure 4. The transmittance of the proposed smart windows at 35 degrees and different values of d_B (**A**) TE/Air, (**B**) TE/water, (**C**) TM/Air, and (**D**) TM/water.

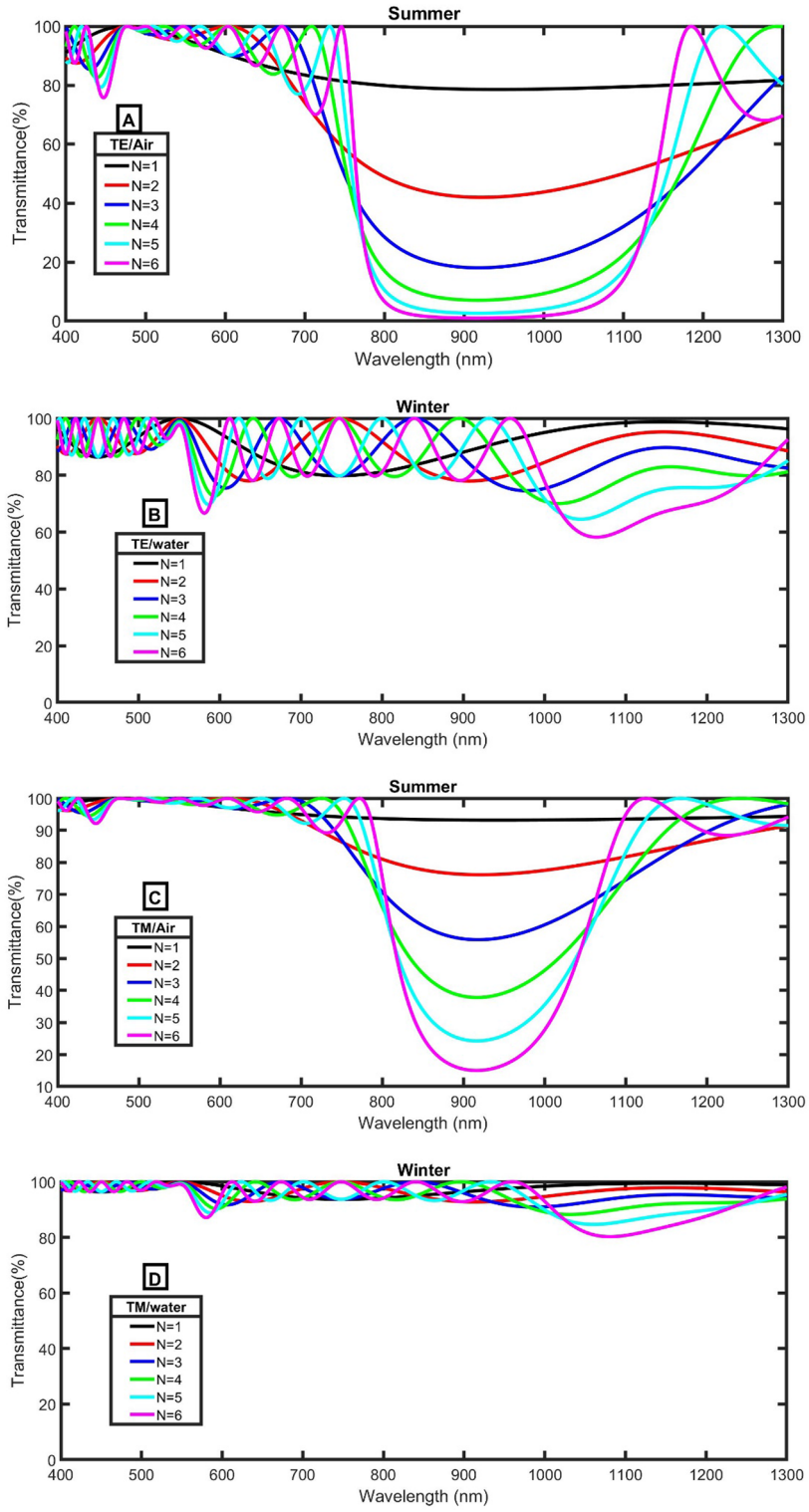

Figure 5. The transmittance of the proposed smart windows at 35 degrees, $d_B = 270$ nm and different values of N (**A**) TE/Air, (**B**) TE/water, (**C**) TM/Air, and (**D**) TM/water.

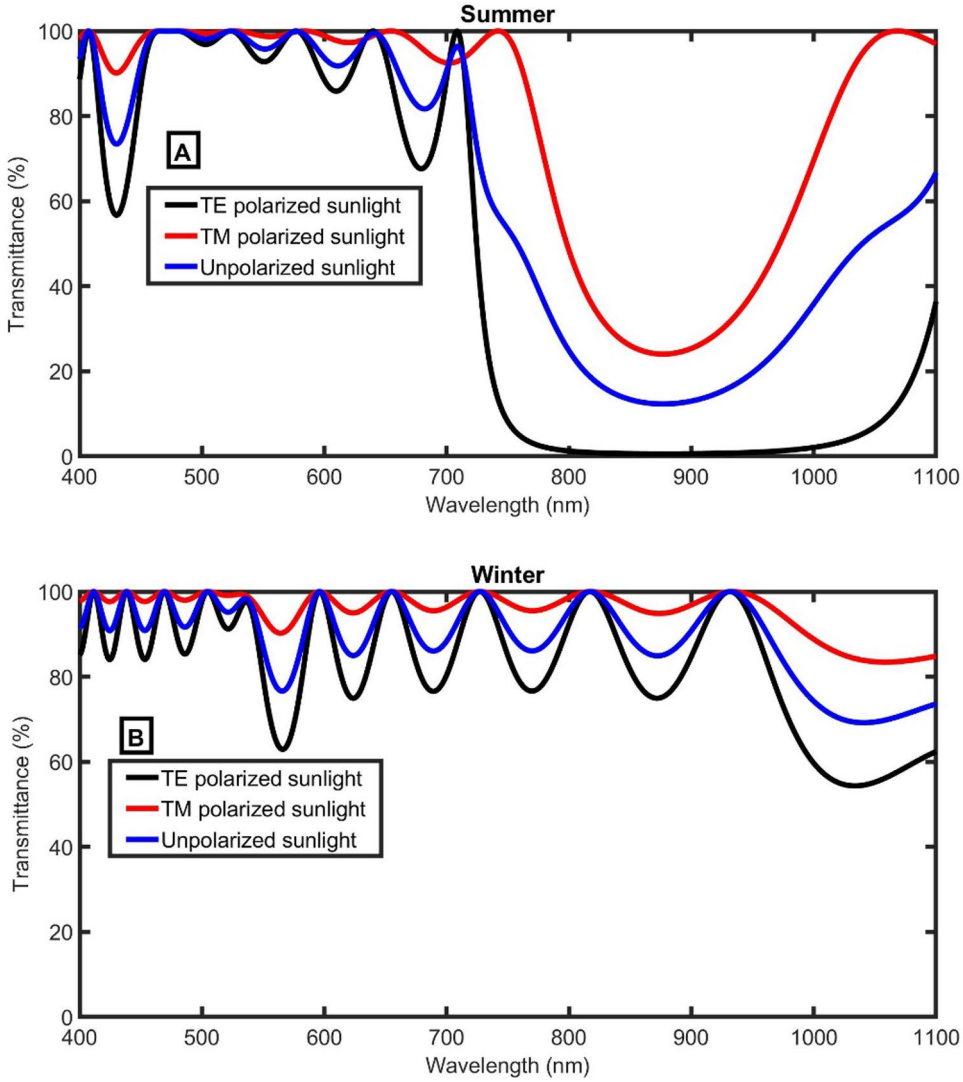

Figure 6. The transmittance of the proposed smart windows at 40 degrees, dB = 270 nm, and N = 6 (**A**) in Summer, and (**B**) in Winter.

Data availability

The datasets used and/or analyzed during the current study are available from the corresponding author on reasonable request.

Received: 15 February 2022; Accepted: 2 June 2022
Published online: 16 June 2022

References

1. Lee, S. G. *et al.* Switchable transparency and wetting of elastomeric smart windows. *Adv. Mater.* **22**, 5013–5017. https://doi.org/10.1002/adma.201002320 (2010).
2. Cao, D., Xu, C., Lu, W., Qin, C. & Cheng, S. Sunlight-driven photo-thermochromic smart windows. *Solar Rrl* **2**, 1700219. https://doi.org/10.1002/solr.201700219 (2018).
3. Wang, S., Gao, W., Hu, X.-Y., Shen, Y.-Z. & Wang, L. Supramolecular strategy for smart windows. *Chem. Commun.* **55**, 4137–4149. https://doi.org/10.1039/C9CC00273A (2019).
4. Davy, N. C. *et al.* Pairing of near-ultraviolet solar cells with electrochromic windows for smart management of the solar spectrum. *Nat. Energy* **2**, 1–11. https://doi.org/10.1038/nenergy.2017.104 (2017).
5. Wang, J.-L., Lu, Y.-R., Li, H.-H., Liu, J.-W. & Yu, S.-H. Large area co-assembly of nanowires for flexible transparent smart windows. *J. Am. Chem. Soc.* **139**, 9921–9926. https://doi.org/10.1021/jacs.7b03227 (2017).
6. Cai, G., Darmawan, P., Cheng, X. & Lee, P. S. Inkjet printed large area multifunctional smart windows. *Adv. Energy Mater.* **7**, 1602598. https://doi.org/10.1002/aenm.201602598 (2017).
7. Zaky, Z. A., Sharma, A. & Aly, A. H. Gyroidal graphene for exciting tamm plasmon polariton as refractive index sensor: Theoretical study. *Opt. Mater.* **122**, 111684. https://doi.org/10.1016/j.optmat.2021.111684 (2021).
8. Zaky, Z. A. & Aly, A. H. Gyroidal graphene/porous silicon array for exciting optical Tamm state as optical sensor. *Sci. Rep.* **11**, 19389. https://doi.org/10.1038/s41598-021-98305-0 (2021).

9. Zaky, Z. A. & Aly, A. H. Modeling of a biosensor using Tamm resonance excited by graphene. *Appl. Opt.* **60**, 1411–1419. https://doi.org/10.1364/AO.412896 (2021).
10. Zaky, Z. A., Sharma, A., & Aly, A. H. Tamm plasmon polariton as refractive index sensor excited by gyroid metals/porous Ta_2O_5 photonic crystal. *Plasmonics* **17**, 681–691 (2021). https://doi.org/10.1007/s11468-021-01559-7
11. Zaky, Z. A., Ahmed, A. M. & Aly, A. H. Remote temperature sensor based on tamm resonance. *SILICON* **14**, 2765–2777. https://doi.org/10.1007/s12633-021-01064-w (2021).
12. Zaky, Z. A., Sharma, A., Alamri, S. & Aly, A. H. Theoretical evaluation of the refractive index sensing capability using the coupling of Tamm-Fano resonance in one-dimensional photonic crystals. *Appl. Nanosci.* **11**, 2261–2270. https://doi.org/10.1007/s13204-021-01965-7 (2021).
13. Aly, A. H., Sayed, H. & Elsayed, H. A. Development of the Monolayer Silicon Solar Cell Based On Photonic Crystals. *SILICON* **11**, 1377–1382. https://doi.org/10.1007/s12633-018-9936-7 (2019).
14. Yablonovitch, E. Photonic crystals: semiconductors of light. *Sci. Am.* **285**, 46–55. https://doi.org/10.1038/scientificamerican1201-46 (2001).
15. Wang, Y., Huang, Q., Zhu, W., Yang, M. & Lewis, E. Novel optical fiber SPR temperature sensor based on MMF-PCF-MMF structure and gold-PDMS film. *Opt. Express* **26**, 1910–1917. https://doi.org/10.1364/OE.26.001910 (2018).
16. Peng, J. *et al.* Thin films based one-dimensional photonic crystal for humidity detection. *Sens. Actuators, A* **263**, 209–215 (2017).
17. Karmakar, S., Kumar, D., Varshney, R. & Chowdhury, D. R. Strong terahertz matter interaction induced ultrasensitive sensing in fano cavity based stacked metamaterials. *J. Phys. D Appl. Phys.* **53**, 415101. https://doi.org/10.1088/1361-6463/ab94e3 (2020).
18. Nayak, C., Aghajamali, A., Alamfard, T. & Saha, A. Tunable photonic band gaps in an extrinsic Octonacci magnetized cold plasma quasicrystal. *Physica B* **525**, 41–45. https://doi.org/10.1016/j.physb.2017.08.075 (2017).
19. Nayak, C., Aghajamali, A. & Saha, A. Double-negative multilayer containing an extrinsic random layer thickness magnetized cold plasma photonic quantum-well defect. *Superlattices Microstruct.* **111**, 248–254. https://doi.org/10.1016/j.spmi.2017.06.041 (2017).
20. Aly, A. H. *et al.* Detection of reproductive hormones in females by using 1D photonic crystal-based simple reconfigurable biosensing design. *Crystals* **11**, 1533. https://doi.org/10.3390/cryst11121533 (2021).
21. Zaky, Z. A., Panda, A., Pukhrambam, P. D. & Aly, A. H. The impact of magnetized cold plasma and its various properties in sensing applications. *Sci. Rep.* **12**, 3754. https://doi.org/10.1038/s41598-022-07461-4 (2022).
22. Zaky, Z. A., Amer, H. A., Suthar, B. & Aly, A. H. Gas sensing applications using magnetized cold plasma multilayers. *Opt. Quant. Electron.* **54**, 217. https://doi.org/10.1007/s11082-022-03594-y (2022).
23. Zaky, Z. A., Singh, M. R., Aly, A. H. Tamm resonance excited by different metals and graphene. *Photon. Nanostruct. Fundam. App.* **49**, 100995 (2022). https://doi.org/10.1016/j.photonics.2022.100995
24. Aly, A. H., Ameen, A. A., Elsayed, H. A., Mohamed, S. & Singh, M. R. One-dimensional metallo-superconductor photonic crystals as a smart window. *J. Supercond. Novel Magn.* **32**, 2313–2318. https://doi.org/10.1007/s10948-018-4978-z (2019).
25. Aly, A. H., Ameen, A. A. & Vigneswaran, D. Superconductor nanometallic photonic crystals as a novel smart window for low-temperature applications. *J. Supercond. Novel Magn.* **32**, 191–197. https://doi.org/10.1007/s10948-018-4716-6 (2019).
26. Aly, A. H., Ahmed, A. M. & Shaban, M. Multilayer angular optical filter as a smart window. *Indian J. Phys.* **94**, 95–103. https://doi.org/10.1007/s12648-019-01438-2 (2020).
27. Gao, L., Lemarchand, F. & Lequime, M. Exploitation of multiple incidences spectrometric measurements for thin film reverse engineering. *Opt. Express* **20**, 15734–15751. https://doi.org/10.1364/OE.20.015734 (2012).
28. Jena, S. *et al.* Omnidirectional photonic band gap in magnetron sputtered TiO2/SiO2 one dimensional photonic crystal. *Thin Solid Films* **599**, 138–144. https://doi.org/10.1016/j.tsf.2015.12.069 (2016).
29. Hale, G. M. & Querry, M. R. Optical constants of water in the 200-nm to 200-µm wavelength region. *Appl. Opt.* **12**, 555–563. https://doi.org/10.1364/AO.12.000555 (1973).
30. Luque-Raigón, J. M., Halme, J. & López-López, C. Angular optical behavior of photonic-crystal-based dye-sensitized solar cells. *J. Photon. Energy* **9**, 025501. https://doi.org/10.1117/1.JPE.9.025501 (2019).
31. Yeh, P. *Optical Waves in Layered Media*: Wiley, New York (1988).
32. Born, M. & Wolf, E. *Principles of Optics: Electromagnetic Theory of Propagation, Interference and Diffraction of Light*. Elsevier (2013).
33. Zaky, Z. A. & Aly, A. H. Highly sensitive salinity and temperature sensor using tamm resonance. *Plasmonics* **16**, 2315–2325. https://doi.org/10.1007/s11468-021-01487-6 (2021).
34. Zaky, Z. A., Aly, A. H. & Moustafa, B. Plasma cell sensor using photonic crystal cavity. *Opt. Quant. Electron.* **53**, 591. https://doi.org/10.1007/s11082-021-03201-6 (2021).
35. Zaky, Z. A., Sharma, A., Alamri, S., Saleh, N. & Aly, A. H. Detection of fat concentration in milk using ternary photonic crystal. *Silicon* (2021). https://doi.org/10.1007/s12633-021-01379-8
36. Zaky, Z. A., Ahmed, A. M., Shalaby, A. S. & Aly, A. H. Refractive index gas sensor based on the Tamm state in a one-dimensional photonic crystal: Theoretical optimisation. *Sci. Rep.* **10**, 9736. https://doi.org/10.1038/s41598-020-66427-6 (2020).

Acknowledgements

The authors thank the reviewers and editors for improving this article.

Author contributions

Z.A.Z. invented the original idea of the study, implemented the computer code, performed the numerical simulations, analyzed the data, wrote and revised the main manuscript text. A.H.A. discussed the results and supervised this work. All Authors developed the final manuscript.

Funding

Open access funding provided by The Science, Technology & Innovation Funding Authority (STDF) in cooperation with The Egyptian Knowledge Bank (EKB). The authors declare no fund.

Competing interests

The authors declare no competing interests.

Additional information

Correspondence and requests for materials should be addressed to Z.A.Z.

Reprints and permissions information is available at www.nature.com/reprints.

Publisher's note Springer Nature remains neutral with regard to jurisdictional claims in published maps and institutional affiliations.